Chinese Journal of Physiology 52(2): 81-92, 2009
DOI: 10.4077/CJP.2009.AMG016

Dynamic Performance Evaluation on the Synergy of Micturition in Spinal Cord-Injured Female Rats under Pharmacological Effects

Shyang Chang[1]*, Shiun-Jeng Li[1], Shih-Jen Hu[1], Hsiu-Yao Cheng[2], Sheng-Hwu Hsieh[3], and Chen-Li Cheng[4]*

[1]*Department of Electrical Engineering, National Tsing Hua University*
Hsinchu 300, Taiwan, ROC
[2]*Department of Chemistry, Tunghai University*
Taichung 407, Taiwan, ROC
[3]*Department of Endocrinology and Metabolism, Chang Gung Memorial Hospital*
Chang Gung University College of Medicine
Taipei 100, Taiwan
and
[4]*Division of Urology, Department of Surgery, Taichung Veterans General Hospital*
Taichung 407, Taiwan, ROC

Abstract

Recently, a temporal "coherent" fractal structure and synchronization of rhythms were proposed as two essential indicators for efficient voiding during micturition in female rats. The former was correlated with the *intensity* and the latter the *frequency* of physiological signals embedded in random noise. Studies using both indices confirmed that synergic co-activations of bladder and external urethral sphincter (EUS) of female rats were present during the voiding of urine. Therefore, it would be interesting to investigate if these two criteria could be used in the performance evaluation of pharmacological effects on spinal cord-injured rats during micturition. In this paper, the primary goals were to (1) examine if the involved muscles in the lower urinary tract would be under similar synergic co-activations during the administration of capsaicin (CAP) and resiniferatoxin (RTX), and (2) characterize quantitatively the differences of their nervous responses simultaneously. A total of 62 micturition experiments were performed on sixteen spinal cord-injured adult female Sprague-Dawley rats, and then the electromyograms of EUS and cystometrograms of bladder were analyzed. Results based on the aforementioned criteria indicated that the synergy of bladder and EUS during micturition by using RTX was better than that of the CAP. Furthermore, the residue urine volumes for rats under the former treatment were smaller than those of the rats under the latter treatment. Consequently, we concluded that the administration of RTX was more effective than CAP in facilitating voiding in the spinal cord-injured rats.

Key Words: capsaicin, dynamical disease, reciprocal innervations, resiniferatoxin, synergy of micturition

Introduction

For many diseases, the normal organization of physiological systems is replaced by abnormal temporal or spatial dynamics. "Dynamical diseases" are used to characterize such abnormal temporal organization

Corresponding author: Dr. Shyang Chang, Department of Electrical Engineering, National Tsing Hua University, Hsinchu 300, Taiwan, ROC. Tel: +886-35731146, Fax: +886-35715971, E-mail: shyang@ee.nthu.edu.tw and Dr. Chen-Li Cheng, Division of Urology, Department of Surgery, Taichung Veterans General Hospital, Taichung 407, Taiwan, ROC. Tel: +886-4-23741215, Fax: +886-4-23593160, E-mail: cheng20011@yahoo.com.tw
*These two authors have equal contribution.
Received: March 26, 2008; Revised: September 7, 2008; Accepted: September 30, 2008.
©2009 by The Chinese Physiological Society. ISSN : 0304-4920. http://www.cps.org.tw

(17). For instance, normal operations of the lower urinary tract to store and void urine rely on the neural regulation of the central nervous system and peripheral nervous system (1, 18). The lower urinary tract usually contains the bladder and external urethral sphincter (EUS), and they are anatomically coupled. During micturition, it is mediated by a spinal reflex pathway, which is organized in the lumbar and sacral regions of the spinal cord (28). In this paper, in order to describe the dynamical behavior of the lower urinary tract, the descriptive term of these two muscle groups being "synchronized" is used to denote that they have the same frequencies. The term of these two groups being "synergic" is used to denote that they have the same frequencies *and* persistent signal intensities (3-5). By investigating the EUS electromyograms (EMG) and bladder cystometrograms (CMG) of intact rats, we find that there is synergy between the bladder and EUS during normal voiding stage (3-5). In determining the synergy, the frequencies of detrusor and EUS are temporally synchronized and their signal intensities are persistent as the fractal dimensions (FDs) being coherently less than 1.5 during voiding. The modalities of the spinal cord-injured (SCI) female rats usually lack either such synchronization or temporal coherence of FDs, and sometimes both (3).

It is usually believed that after spinal cord injury, the C fiber afferents must be strengthened. Therefore, it accounts for the development of overactive bladder and at least in part for detrusor-sphincter dyssynergia (2, 20, 22, 26, 27). Capsaicin (CAP) and resiniferatoxin (RTX) are two specific nerve inhibitors to C-fiber afferents (9, 10, 16, 21). The drug administration of CAP or RTX is believed to achieve significant improvement of detrusor hyperreflexia and dyssynergia (2, 11, 15, 16, 21).

In this paper, we will administer CAP and RTX to two groups of SCI rats and evaluate the dynamic performance of micturition for each pharmacological therapy. To assess the pharmacological effects of these two different drug treatments on voiding efficacy, we invoked both the FDs and time-frequency analysis to evaluate if there was any synergic coactivation of SCI rats during micturition (3-6, 12-14, 19, 23, 24, 29-31). The results would be helpful for physiologists to assess the curative power of pharmacological therapies in animal studies.

Materials and Methods

Experimental Procedures

A total of 62 micturition experiments were performed on sixteen SCI adult female Sprague-Dawley rats, weighing 250-400 grams. Spinal transection at T_9-T_{11} vertebral bone was performed under halothane anesthesia. Gel foam was placed between the severed ends of the spinal cord. After the overlying muscle and skin were sutured, the rats were treated with antibiotics (ampicillin 150 mg/kg, intramuscularly) for 8-10 days. To prevent over distension of the bladder, urine was manually expressed every 6-8 h until automatic micturition was developed 7 to 12 days postsurgery. Then, the bladder was manually expressed two to three times per day. The level of spinal transection was histologically confirmed postmortem after experiments. The Institutional Animal Care and Use Committee of the Taichung Veterans General Hospital approved the protocol used in this study.

After spinal transection, all SCI rats were examined 6-8 weeks and then were pre-treated with RTX (1,000 nM, intravesically) or CAP (125 mg/Kg, subcutaneously) by dividing into consecutive days. The urodynamic experiments were then performed 4 days later. The vehicle of RTX consists of 10% ethanol, 10% Tween 80, and 80% physiological saline. As for CAP, it was administered in a solution containing 20 mg/ml CAP in a vehicle containing 10% ethanol, 10% Tween 80, and 80% physiological saline. The 0.3 ml of RTX solution was injected into the bladder and was kept inside the bladder for 2 h. The solution was drained after the intravesical treatment. Among these sixteen SCI rats, six were administrated with RTX, five with CAP and five without any drug administration as the controls. Hereafter, the SCI rats with RTX treatment would be denoted as RTX rats, the SCI rats with CAP treatment as CAP rats, and the SCI rats without any drug treatment simply as SCI rats.

Micturition experiments proceeded as follows. The rats were first anesthetized with urethane (0.72 g/kg, subcutaneously). A tracheal tube was inserted so the rat could be placed on a ventilator to facilitate respiration as usual. Arterial blood pressure was measured by attachment of a pressure transducer connected to a cannula in the common carotid artery. All urodynamic investigations were performed on a surgically exposed urinary tract and bladder *via* a middle abdominal incision. The rostral half of pubic symphysis was removed to expose the middle urethra and EUS. The EUS defined here indicated the striated sphincter muscle surrounding the urethra. Two fine insulated silver wire electrodes (0.05 mm diameter) with exposed tips were inserted into lateral sides of midurethra where muscle fibers of the EUS were identified.

A polyethylene tube was inserted into the apex of the bladder dome through one small incision. To detect the intravesical pressure and infuse physiological saline into the bladder, the polyethylene tube was connected *via* a 3-way stopcock to a pressure

transducer and an infusion pump. The infusion rate was set at 0.123 ml/min. The CMGs were then measured under infusing saline solutions at room temperature. After completion of the micturition experiments, the residual urine was removed from the bladder and measured.

Data Acquisition

The CMG and EUS EMG activities were recorded and then sampled *via* the MP100WSW system at rate 500 points/sec. The signals were filtered with band-stop of 60 Hz to eliminate power line interference. In fact, the EMG activity of female rats during micturition was below 50 Hz. Hence, the sampling rate 500 points/sec was high enough for this experiment. Among these three groups of adult female rats used in our micturition experiments, 20 contractions of six RTX rats, 18 contractions of five CAP rats, and 24 contractions of five SCI rats were then analyzed.

The Mathematical Model

The rationale behind our modeling was presented in various previous works (3-8). The model could be traced back to the Brownian motion observed by R. Brown. According to N. Wiener, the Brownian motion $\{B(t),\ t \geq 0\}$ was defined as the formal integral of the random series of oscillations, such as $\int_0^t \sum_{n=-\infty}^{\infty} \xi_n e^{inx} dx$, where $\{\xi_n\}$, which is a sequence of independent, identically distributed standard complex Gaussian random variables (25). He then proves that this integral converged both in the L^2 sense and almost surely. However, the increments of Brownian motion are independent, Benoit B. Mandelbrot proposes in 1968 the so-called fractional Brownian motion with "correlated" increments for practical applications. The fractional Brownian motion (FBM) $\{B_H(t),\ t \geq 0\}$ with Hurst parameter H and starting value b_0 at time 0 was defined by him as $B_H(0) = b_0$, and

$$B_H(t) - B_H(0) = \frac{1}{\Gamma(H+1/2)} \left\{ \int_{-\infty}^{0} [(t-s)^{H-1/2} - (-s)^{H-1/2}] dB(s) + \int_0^t (t-s)^{H-1/2} dB(s) \right\}. \quad (1)$$

The increments of this FBM are now still stationary but dependent. In most applications, data were always sampled in discrete-time format. Hence, the discrete-time fractional Gaussian noise (FGN) process $\{x_H[n]\}$ could be defined as the increment of sampled FBM. That is,

$$x_H[n] = B_H[n] - B_H[n-1], \quad (2)$$

where $B_H[n] = B_H(nT_s)$ and T_s is the sampling period. The autocorrelation function of discrete-time FGN process, denoted by $r_H[k]$, could be evaluated by the following formula:

$$E(x_H[n+k]x_H[n]) \equiv r_H[k] = \frac{1}{2}(|k+1|^{2H} - 2|k|^{2H} + |k-1|^{2H}). \quad (3)$$

From these definitions, it is fitting that the discrete-time FBM and FGN can be used to model the collective behavior of muscle fibers exhibiting different oscillation frequencies with or without correlated amplitudes.

Since sampled EMG signals consist of noise-like activity and sampled CMG signals reflect the cumulative effect from smooth muscles of the bladder, they can be modeled as discrete-time FGN and discrete-time FBM, respectively (3-5, 7, 8). If we take the difference of the sampled CMG, it then becomes the discrete-time FGN process. Notice that the discrete-time EMG signals and differenced CMG signals in our application are not stationary in the long-term, but they are wide-sense stationary in the short-term or during different phases of micturition. For instance, the bursting period of micturition usually lasts 3~4 seconds, hence the signals of 1-second duration can be treated as short-term stationary. Hence, it is fitting for us to use time-frequency analysis and fractal dimension estimation under proper window size in these non-stationary time series. Consequently, we will estimate FDs and spectral frequencies for both EMG and (differenced) CMG time series to extract physiological and pathological features of all three groups of rats in our micturition experiments. The detailed mathematical derivations of the estimations of FD and spectral frequencies in our time-frequency analysis are summarized in the Appendices A, B, and C, and more details can be found in (3-5, 7, 8).

The meanings of FD in physiological signals can be understood as follows. First of all, it can give us an indication about the persistency of the "signal intensity". The reasons are as follows. The variance function of FBM is denoted by $\langle (B_H(t))^2 \rangle \sim t^{2H}$ assuming $B_H(0) = 0$ almost surely. Here the term $\langle (B_H(t))^2 \rangle$ is equivalent to the average "signal intensity," and it is proportional to H and the FD is denoted by $D = 2 - H$. For instance, for Brownian motion of stationary and independent increments, the value of H is 0.5 and $D = 1.5$. According to our studies, if the muscle groups are at rest, then the values of H are usually around 0.5 (3, 4). It indicates that the

muscle fibers are rather independent and not correlated. If H is greater than 0.5, *i.e.*, $1 < D < 1.5$, the integrated effect of muscle groups can be categorized as positively correlated or persistent. In this case, the two different muscle groups have strong and bursting signal amplitudes. If D is between 1.5 and 2, the corresponding effect can be categorized as negatively correlated or antipersistent (3-5, 7, 8, 14, 24). Similarly, the autocorrelation function of discrete-time FGN is also proportional to H according to equation (3). It is also proportional to signal intensity as indicated in (31). Hence, D can also be used as an indicator of the persistence of "signal intensity" in the FGN case. Secondly, the FD can be used as one indicator for dynamical synergy in physiology when combined with spectral frequency (3-5, 7, 8).

Analysis Method for EMG and CMG Signals

Time courses of the estimated FD and spectral frequency were represented in color codes. These colored pictures of spectral frequency and FD were used as diagnostic tools for all three groups of rats in our micturition experiments. Both estimations were based on the spectral distribution function (SDF) idea *via* Bochner's theorem (3, 4, 5, 7, 8, 12, 19, 30, 31). The flowchart of creating these color-coded pictures was shown in Fig. 1. The steps in Fig. 1 were explained as follows:

Step 1. Take the difference if the signal $x[n]$ is CMG, and use the original $x[n]$ if it is EMG.
Step 2. Calculate FD and spectral frequency for the window size of 1 sec, or 500 points of $x[n]$.
Step 3. Estimate the autocorrelation function of the signal and then its SDF $\hat{F}(\lambda)$.
Step 4. Obtain spectral frequency by taking the difference on the sampled SDF.
Step 5. Represent $F(\lambda)$ by Legendre polynomials (LPs) and then find D *via* a database which is established on the autocorrelation function $r_H[k]$ of discrete-time fractional Gaussian noise.
Step 6. Go to Step 2 and shift the processing window one point to the right until the window have covered the last 500 points of the time series.
Step 7. Represent the results with color codes.

Remark: In Step 5, the LPs were used as the fundamental bases for the construction of database. The details were explained in Appendices B and C. The number of terms for LP was usually small. For instance, 5 terms were already enough for estimating the FDs. The improvement of the mean and standard deviation of FD estimates was not significant when

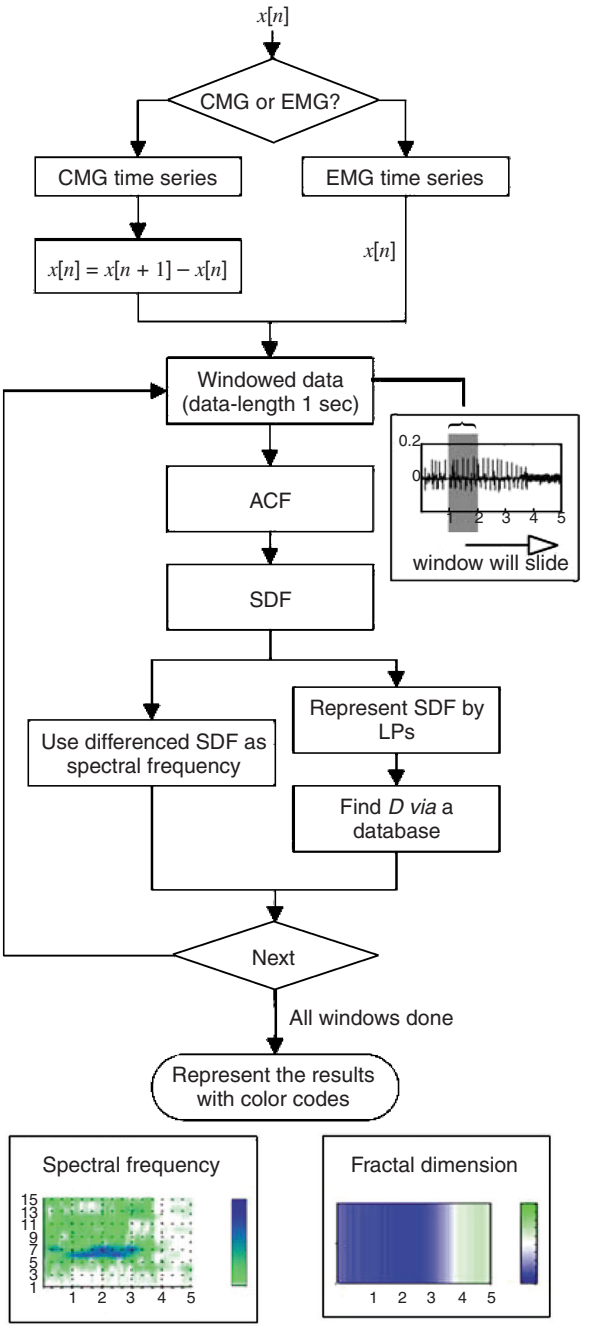

Fig. 1. The flowchart in the analysis of EMG and CMG signals.

larger terms such as 6, 7, ... 20, were used. In Step 7, the values of FDs were between 1 and 2. We encoded different values of FD with different gray levels by the following color code. For instance, it would be encoded in green color if the value was 2. Similarly, the value of 1.5 was coded in white, and the value of 1 in blue. As for the magnitudes of spectral frequencies, they were in normalized units (n.u.). The smallest value 0 was coded in white color and other low values in green. The maximum magnitude was

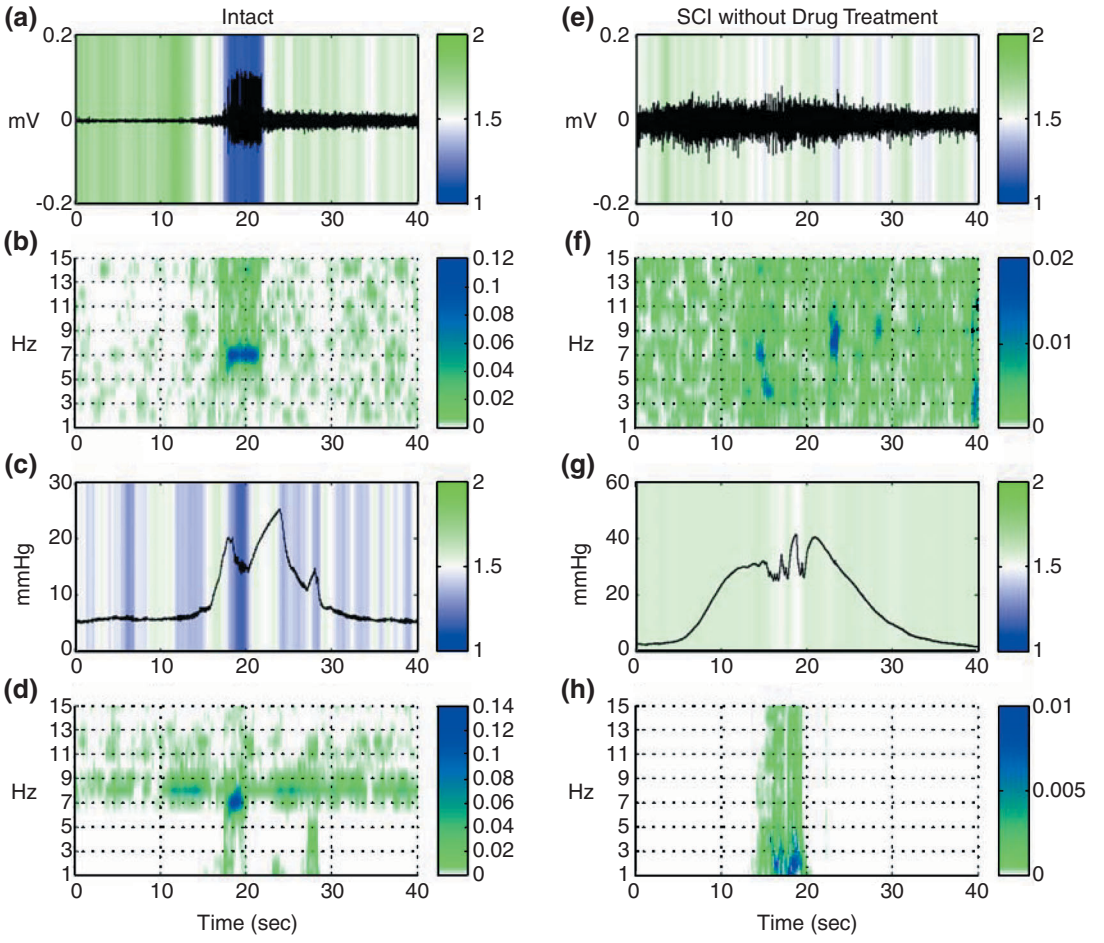

Fig. 2. EMG, CMG, corresponding FDs and spectral frequencies of one complete cycle for an intact rat and a SCI rat. EMG and CMG signals are plotted by black curves and their corresponding FDs and spectral frequencies are coded according to the color bar on their righthand sides. Figs. (a)-(d) are for the intact rat while Figs. (e)-(h) are for the SCI rat. (a) EMG signal and its respective FDs in color code. (b) Time-frequency map for EMG. (c) CMG signal and its respective FDs in color code. (d) Time-frequency map for CMG. (e) EMG and its respective FDs in color code. (f) Time-frequency map for EMG. (g) CMG signal and its respective FDs in color code. (h) Time-frequency map for CMG.

denoted as Cmax and coded in blue.

Results

In storage phase, the bladder was filled with urine and would initiate the voiding desire when the intravesical pressure reached up to a threshold. As the experiments proceeded, these two phases, storage and voiding phases, would be repeated. Figs. 2 and 3 demonstrated just one complete storage and voiding cycle. For clarity and comparison, the EMG and CMG signals of intact rats were also included in Fig. 2. In general, the signals for different cycles in the same female rat were similar with only minor variations among the cycles. For different rats, the variations were certainly much greater. Their FDs were presented in Tables 1, 2, and 3. The intra- and inter-animal variations were explained later in the Discussion section.

Fig. 2 demonstrated the EMG and CMG signals and their resultant characteristics of an intact rat and an SCI rat. There were eight subplots in this figure. Figs. 2(a)-2(d) were for the intact rats while Figs. 2(e)-2(h) were for the SCI rats. The illustration of the intact rats was for comparison only. The EMG and CMG signals were depicted in black curves as in Figs. 2(a) and 2(c) and their respective FDs were displayed by color stripes with a color bar on the right-hand side. In Figs. 2(b) and 2(d), the time-frequency maps of EMG and CMG were displayed aligned with the signals. The Cmax of Fig. 2(b) was 0.12 and the Cmax of Fig. 2(d) was 0.14.

First of all, in Fig. 2(a), the voiding phase could be identified by inspecting the original EMG signals. The higher voltage of EMG bursting signals could be easily seen from 18 sec to 22 sec. Similarly, in Fig. 2(c), the bladder pressure was raised to a higher value over the threshold about 20 mmHg and an oscillatory variation in pressure from 18 sec to 21 sec could

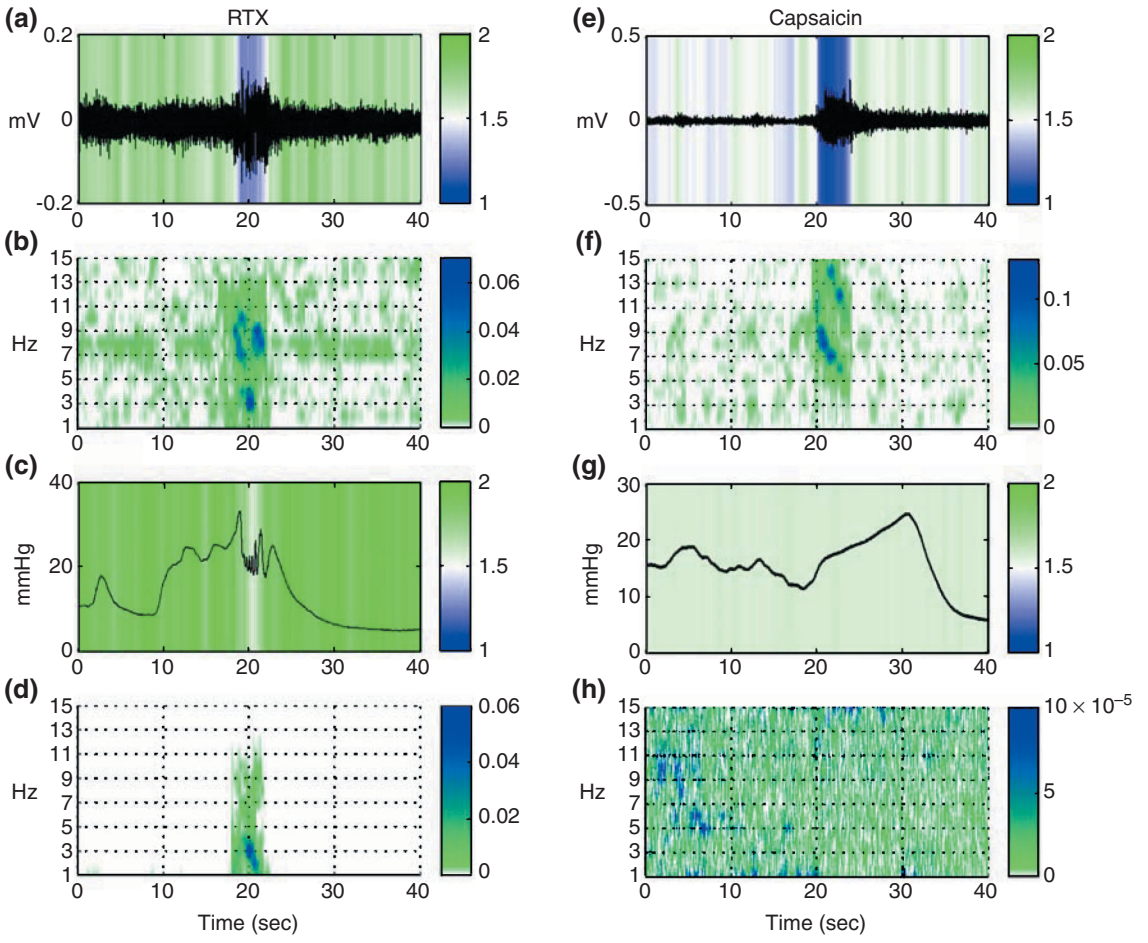

Fig. 3. EMG, CMG, corresponding FDs and spectral frequencies of one complete cycle for an RTX rat and a CAP rat. EMG and CMG signals are plotted by black curves and their corresponding FDs and spectral frequencies are coded according to the color bar on their righthand sides. Figs. (a)-(d) are for the RTX rat while Figs. (e)-(h) for the CAP rat. (a) EMG signal and its respective FDs in color code. (b) Time-frequency map for EMG. (c) CMG signal and its respective FDs in color code. (d) Time-frequency map for CMG. (e) EMG and its respective FDs in color code. (f) Time-frequency map for EMG. (g) CMG signal and its respective FDs in color code. (h) Time-frequency map for CMG.

be observed. In Fig. 2(b), the spectral frequency of Fig. 2(a) was computed and the blue spot around the 7 Hz (from 18 sec to 22 sec) illustrated the strong rhythmic contraction of the EUS during the voiding phase. More precisely, the 7 Hz component at 18.33 sec of EMG had the maximum power 0.12 n.u. In Fig. 2(d), the blue spot around 7Hz (from 18 sec to 20 sec) illustrated the strong rhythmic contraction of bladder during the voiding phase. The 7 Hz component at 18.6 sec of CMG had the maximal power 0.14 n.u.. This result clearly indicated that these two muscle groups were synchronized.

Secondly, in Fig. 2(a), the values of the region of low FDs (18 sec to 22 sec) for EMG were below 1.2 and were denoted by the blue stripes. In Fig. 2(c), the values of the region of low FDs (18 sec to 20 sec) for CMG were below 1.4 and were denoted by the light blue stripes. To compare the FDs, the mean value of FDs for EMG in a 4-sec interval during voiding phase was denoted by μ_{FD_EMG} and the corresponding mean value of FD for CMG by μ_{FD_CMG}. Here, μ_{FD_EMG} was 1.188 and μ_{FD_CMG} 1.374. Hence, both signals had temporal "coherent" fractal structure. Combining the results of FDs and spectral frequencies, we could see that this intact rat was in synergy during micturition.

As for the SCI rats, Figs. 2(e)-2(h) indicated that it was not easy to distinguish the voiding phase from the non-voiding phase even though the voiding phase was estimated to be between 15 and 25 sec from Fig. 2(g). The Cmax of Fig. 2(f) was 0.02; the Cmax of Fig. 2(h) was 0.01. In Fig. 2(f), the significant frequency component of EMG was noticeable around 8 Hz with the maximum magnitude 0.02 n.u.. Note that these values were rather small, as compared with those of the intact rats. In Fig. 2(h), except for the 1 Hz low frequency component with 0.01 n.u., there were no other significant frequency components in

Table 1. The mean FDs in three stages of EMG and CMG for six RTX rats. For a given specific contraction, the values in *italics* and boldface are the smallest mean FD of EMG and CMG in three stages. The last two rows, "Avg" and "Std", are the average and standard deviation of the total 20 contractions

Rat No.	Exp. No.	EMG (FD)			CMG (FD)		
		Before voiding	During voiding	After voiding	Before voiding	During voiding	After voiding
Rat 1	1	1.704	***1.334***	1.700	1.856	***1.712***	1.927
Rat 1	2	1.672	***1.454***	1.704	1.946	***1.798***	1.920
Rat 1	3	1.647	***1.424***	1.708	1.949	***1.897***	1.953
Rat 2	4	1.441	***1.142***	1.481	1.890	***1.764***	1.886
Rat 2	5	1.247	***1.085***	1.409	1.918	***1.748***	1.919
Rat 2	6	1.267	***1.242***	1.425	1.882	***1.793***	1.926
Rat 2	7	1.267	***1.063***	1.235	1.918	***1.613***	1.924
Rat 3	8	1.595	***1.107***	1.548	1.990	***1.916***	1.988
Rat 3	9	1.602	***1.100***	1.438	1.781	***1.761***	1.994
Rat 3	10	1.593	***1.122***	1.584	1.929	***1.869***	1.966
Rat 3	11	1.593	***1.117***	1.564	1.981	***1.811***	1.995
Rat 3	12	1.601	***1.144***	1.552	1.999	***1.951***	1.972
Rat 4	13	1.581	***1.111***	1.612	1.999	***1.885***	1.999
Rat 4	14	1.619	***1.067***	1.559	1.999	***1.748***	1.982
Rat 4	15	1.393	***1.071***	1.604	1.983	***1.927***	1.999
Rat 4	16	1.341	***1.044***	1.396	1.999	***1.938***	1.999
Rat 5	17	1.048	***1.023***	1.045	1.759	1.763	***1.748***
Rat 5	18	1.100	***1.021***	1.117	1.759	***1.741***	1.788
Rat 6	19	1.507	***1.137***	1.652	1.861	***1.728***	1.830
Rat 6	20	1.475	***1.218***	1.636	1.816	***1.783***	1.860
Avg		1.465	***1.151***	1.498	1.911	***1.807***	1.929
Std		0.194	0.124	0.187	0.083	0.090	0.073

CMG. In Fig. 2(e), the narrow region of low FDs for EMG centered around 23 sec, but, in Fig. 2(g), the region of low FDs for CMG was between 15 sec and 20 sec. Moreover, inside this period, μ_{FD_CMG} was 1.531 and μ_{FD_EMG} 1.543. Combining the results of FDs and spectral frequencies, we concluded that the SCI rat had no synergy at all during micturition.

Fig. 3 demonstrated the EMG and CMG signals and their resultant characteristics of a typical RTX rat and a CAP rat. We first examined the behavior of RTX rat in Figs. 3(a) and 3(c). From the time series of EMG and CMG, it was obvious that the voiding phase was around 20 sec. The Cmax of Fig. 3(b) was 0.07; the Cmax of Fig. 3(d) was 0.06. In Fig. 3(b), the 3 Hz component on 20.1 sec had maximal power 0.07 n.u.. In Fig. 3(d), the 3 Hz component on 20 sec had maximal power 0.06 n.u..

In Fig. 3(a), the region of low FDs for EMG was between 18 sec to 21 sec, and during this period the FDs were below 1.4. The value of μ_{FD_EMG} was 1.334 inside this period. In Fig. 3(c), the region of low FDs for CMG decreased around 20 sec. However, during this period the FDs were not below 1.5. The value μ_{FD_CMG} was actually 1.712 inside this period.

As to the CAP rat in Fig. 3(e), the bursting electrical signals between 20 and 25 sec were easily identified as the voiding phase. In Fig. 3(g), the CMG showed that this CAP rat had no clear alteration of the bladder pressure over the threshold. The Cmax in Fig. 3(f) was 0.13 and the Cmax in Fig. 3(h) was 0.0001. In Fig. 3(f), the blue color region of 6 ~ 8 Hz lasted from 20 sec to 23 sec and the 8 Hz component with maximal magnitude 0.13 n.u. was at 20.8 sec. In Fig. 3(h), there was no significant frequency component of CMG in the whole cycle.

In Fig. 3(e), the region of low FDs for EMG was between 20 sec to 24 sec, and during this period the FDs were below 1.4. Moreover, μ_{FD_EMG} was 1.215 inside this period, while in Fig. 3(g), the region of low FDs for CMG was not obvious between 20 sec and 24 sec. Its μ_{FD_CMG} was 1.572.

To further distinguish the RTX rats from CAP rats, the statistics of mean FDs of EMG and CMG were illustrated in Tables 1, 2, and 3. For example, the "Avg" and "Std" of the last two rows in Tables 1 and 2 indicated the average value and standard deviation of all the contractions under RTX and CAP treatment, respectively. The average value and stan-

Table 2. The mean FDs in three stages of EMG and CMG for five CAP rats. For a given specific contraction, the values in *italics* and boldface are the smallest mean FD of EMG and CMG in three stages. The last two rows, "Avg" and "Std", are the average and standard deviation of the total 18 contractions

Rat No.	Exp. No.	EMG (FD)			CMG (FD)		
		Before voiding	During voiding	After voiding	Before voiding	During voiding	After voiding
Rat 7	1	1.349	***1.345***	1.548	1.587	1.588	***1.583***
Rat 7	2	1.432	***1.278***	1.535	1.598	***1.581***	1.599
Rat 7	3	1.391	***1.135***	1.569	1.599	***1.592***	1.598
Rat 8	4	1.574	***1.474***	1.608	1.563	***1.557***	1.561
Rat 8	5	1.538	***1.377***	1.553	***1.560***	***1.560***	1.563
Rat 8	6	***1.469***	1.561	1.561	***1.560***	1.562	1.563
Rat 9	7	***1.497***	1.530	1.503	***1.638***	1.639	1.649
Rat 9	8	***1.479***	1.529	1.485	1.665	***1.637***	1.655
Rat 9	9	***1.484***	1.568	1.521	1.667	***1.637***	1.658
Rat 10	10	1.300	***1.280***	1.346	1.570	***1.558***	1.559
Rat 10	11	1.299	***1.269***	1.337	1.563	***1.548***	1.561
Rat 10	12	1.344	***1.247***	1.332	1.563	1.562	***1.552***
Rat 10	13	1.296	***1.238***	1.329	1.577	1.563	***1.557***
Rat 10	14	1.298	***1.230***	1.329	1.574	***1.557***	1.571
Rat 11	15	1.462	***1.347***	1.569	***1.593***	1.595	1.602
Rat 11	16	1.465	***1.215***	1.550	***1.566***	1.572	1.570
Rat 11	17	1.351	***1.220***	1.473	***1.575***	1.576	1.577
Rat 11	18	1.379	***1.222***	1.466	1.596	1.587	***1.582***
Avg		1.412	***1.337***	1.479	1.590	***1.582***	1.587
Std		0.089	0.138	0.099	0.034	0.029	0.034

dard deviation of mean FDs for intra-animal variations were listed in Table 3. The mean values of FD in Tables 1 and 2 were calculated using 4-second intervals for three stages: before, during, and after voiding. There were 20 micturition contractions for the six RTX rats and 18 for the five CAP rats. We compared only the FDs in EMG and CMG because the CAP rats usually had no significant frequencies for comparison. In all the Tables, the values in *italics* and boldface were used to denote the smallest value among the three different stages.

Discussion

In previous studies, we have reached the conclusion that for intact rats, the frequencies of EUS and detrusor of the bladder are synchronized around 7 Hz, and their FDs are temporally "coherent" under 1.5 during voiding to facilitate the micturition process (3, 4). In Fig. 2, this result was included for comparison. The synchronization around 7 Hz of the EUS and the detrusor are depicted in Figs. 2(b) and 2(d) for reference. The results of FDs and spectral frequencies hence implied that, for the intact rats, the bladder and EUS were in synergy during micturition. A possible physiological significance for the 7 Hz and FDs is that the conventional belief in the antagonism of reciprocal innervations (1) shall be replaced by the concept of synergic co-activation between the bladder and EUS.

For the SCI rats, Fig. 2(f) is full of green color code and this phenomenon indicates that there is no clear spectral characteristic except a weak 8 Hz of EMG around 23 sec. In Fig. 2(h), the weak 1Hz component of CMG is not in rhythmic synchronization with the EUS. Furthermore, the FDs of EMC and CMG are not temporally coherent. Hence, the synergy of the EUS and the detrusor is absent in this SCI rat.

In the RTX rat of Figs. 3(b) and 3(d), there is weak synchronization of the rhythms of detrusor and the EUS around 3 Hz with small magnitudes. In Figs. 3(a) and 3(c), the region of low FDs for EMG coincides with that of CMG. This can be confirmed from the FDs of EMG and CMG around 20 sec. This coherent pattern is weaker than that of the intact rats. The reason for that is because the mean FD for EMG is 1.334, but that for CMG is 1.712. Hence, we can see that the RTX rat has "weak" synergy during voiding due to the "weak" synchronization of rhythms and "weak" coherence of FDs.

In Figs. 3(e) and 3(f), for this CAP rat, the EMG signals with respective power spectra and the FDs

Table 3. The average and standard deviation of the mean FDs in three stages of EMG and CMG. Rats 1 to 6 are RTX rats and Rats 7 to 11 are CAP rats. For a given specific rat, the values in *italics* and boldface are the smallest average of mean FDs of EMG and CMG in three stages. The "Avg" and "Std" stand for the average and standard deviation

Rat No.		EMG (FD)			CMG (FD)		
		Before voiding	During voiding	After voiding	Before voiding	During voiding	After voiding
Rat 1	Avg	1.674	***1.404***	1.704	1.917	***1.802***	1.933
	Std	0.029	0.062	0.004	0.053	0.093	0.017
Rat 2	Avg	1.306	***1.133***	1.388	1.902	***1.730***	1.914
	Std	0.091	0.080	0.106	0.019	0.080	0.019
Rat 3	Avg	1.597	***1.118***	1.537	1.936	***1.862***	1.983
	Std	0.004	0.017	0.057	0.091	0.077	0.013
Rat 4	Avg	1.484	***1.073***	1.543	1.995	***1.875***	1.995
	Std	0.137	0.028	0.101	0.008	0.087	0.009
Rat 5	Avg	1.074	***1.022***	1.081	1.759	***1.752***	1.768
	Std	0.037	0.001	0.051	0.000	0.016	0.028
Rat 6	Avg	1.491	***1.178***	1.644	1.839	***1.756***	1.845
	Std	0.023	0.057	0.011	0.032	0.039	0.021
Rat 7	Avg	1.391	***1.253***	1.551	1.595	***1.587***	1.593
	Std	0.042	0.107	0.017	0.007	0.006	0.009
Rat 8	Avg	1.527	***1.471***	1.574	1.561	***1.560***	1.562
	Std	0.053	0.092	0.030	0.002	0.003	0.001
Rat 9	Avg	1.487	***1.542***	1.503	1.657	***1.638***	1.654
	Std	0.009	0.022	0.018	0.016	0.001	0.005
Rat 10	Avg	1.307	***1.253***	1.335	1.569	***1.558***	1.560
	Std	0.021	0.021	0.007	0.006	0.006	0.007
Rat 11	Avg	1.414	***1.251***	1.515	1.583	***1.583***	1.583
	Std	0.058	0.064	0.053	0.014	0.010	0.014

are similar to those of the RTX rats. In contrast, in Figs. 3(g) and 3(h), the CMG signals and the respective power spectra and FDs are quite different from those of the RTX rats. The detrusor exhibits neither significant frequency component nor apparent region of low FDs for CMG. Hence, even though the EUS of the CAP rat contracts around 7-9 Hz as that of the RTX rat, it is not coordinated with the CMG signals. As a result, there is no rhythmic synchronization and temporal coherence in FDs due to the abnormal bladder. It is clear from our standards that the performance of CAP rat is inferior to RTX rats in these exemplary cycles.

Finally, to make sure that RTX rats are really superior to CAP rats in synergy of micturition, 20 contractions of six RTX rats are illustrated in Table 1, and 18 contractions of five CAP rats are shown in Table 2. Here, the mean FDs of EMG and CMG were used in these two Tables. In Table 1, we can see that out of 20 contractions, all 20 have the smallest mean FDs of EMG signals during voiding, and 19 smallest mean FDs of CMG signals during voiding except one after voiding. Note that in the last two rows of Table 1, the average value and standard deviation of mean FDs in 20 contractions are calculated. The average value of mean FDs during voiding phase for EMG is 1.151 for RTX rats. It indicates a significant drop, as compared to the value of 1.465 before voiding and 1.498 after voiding stage. As to the CMG, the average value is 1.807 for voiding phase as compared to the other two values: 1.911 and 1.929. Even though it is not as significant as that of the EMG, the value in voiding phase is still smaller than the other two stages. These results indicated that RTX rats have exhibited significant improvement in the EUS performance and rather weak synergy between the EUS and bladder. This conclusion was obtained by the quantitative characterization of weak synchronization of the frequency around 3 Hz and slight temporal coherence in FDs. As to the 18 contractions of the CAP rats in Table 2, only 14 smallest mean FDs of EMG signals occur during voiding and 9 smallest mean FDs of CMG signals occur during voiding. Hence, CAP rats have exhibited less coordination as compared to the RTX rats according to our quantitative standards. Notice that for CAP rats, the average value (1.337) of mean

EMG FDs during voiding phase has a minor drop as compared to the value of 1.412 before and 1.479 after voiding stage. As for CMGs, the average value is 1.582 during voiding phase as compared to the other two values: 1.590 and 1.587. These three values are almost of the same order. Hence, the pharmacological effect is almost insignificant for the bladders of CAP rats. These results have indicated that CAP rats exhibit only minor improvement in the EUS performance and no synergy between the EUS and bladder. For different cycles of the same rat, there might be minor variations in FDs. For different rats, the inter-animal variations in FDs are certainly much greater. These variations in FDs are listed in Table 3. For instance, the average value of FDs for rat 1 during voiding stage is around 1.404 and that for rat 2 is around 1.133. Similarly, other stages have similar phenomena as can been seen from Table 3.

As to the residual urine (RU) volumes, RU values for six RTX rats are 0.5, 0.5, 0.18, 0.4, 0.5, and 0.45 ml, respectively. The mean and standard deviation of these values are 0.422 and 0.125 ml, respectively. The RU values for five CAP rats are 0.7, 0.4, 0.4, 0.9, and 1.6 ml, respectively. The mean and standard deviation of these five values are 0.800 and 0.495 ml, respectively. The mean and standard deviation of the amounts of RU volume for RTX rats are both smaller than those of the CAP rats. This experimental result is definitely an important piece of information in supporting our performance evaluation methodology.

The CAP and RTX are known to be effective in the C-fiber desensitization by targeting TRPV1 receptors. Clinical studies have also indicated that bladder hyperreflexia after spinal cord injury is also related in part to unmyelinated C-fiber. In this study, the reasons why the results in CAP and RTX-treated rats are different may be twofold. One possibility is that two methods desensitize the different population of afferent C-fibers. Another possibility is that the potency of RTX is greater than CAP, hence pudendal and parasympathetic innervations are more synergic in RTX rats than CAP rats during micturition. Further study in this direction will be important in the future.

In conclusion, we have successfully used temporal coherence of FDs and synchronization of frequencies as two indicators in the quantitative characterization of dynamic performance evaluation on the pharmacological efficacy of RTX and CAP during the micturition of SCI rats. Our results have revealed that the rats under RTX have weak synergy, as compared to no synergy for rats under CAP. Furthermore, the RU volumes for RTX rats are smaller than those of the CAP rats. Hence, the administration of RTX for SCI rats seems to be more effective in facilitating voiding than CAP. It is believed that the proposed method can be helpful in the performance evaluation of pharmacological effects, especially for dynamical diseases.

Appendix A: Bochner's Theorem and SDF

The estimations of both FDs and spectral frequencies are based on the SDF idea *via* Bochner's theorem (3, 4, 7, 8, 30, 31). The physiological signals can sometimes be modeled as wide sense stationary processes. Without loss of generality, the stationary processes can also be assumed as zero mean so that the covariance functions are the same as autocorrelation functions (ACFs). Since the ACF of discrete-time fractional Gaussian noise is not square-summable, it is not possible to define the power spectral density of such noise by the Fourier transform of its ACF. However, the SDF is still well-defined and it will be used in this paper. According to Bochner's theorem, a continuous ACF denoted by $R(\cdot)$ will induce a spectral measure which is denoted by $F(\cdot)$ on the real line. For F defined on intervals with continuous endpoints, it takes the following form:

$$F([a, b]) = \lim_{n \to \infty} \int_{-\infty}^{\infty} R(\tau) \frac{e^{-i2\pi\tau b} - e^{-i2\pi\tau a}}{-i2\pi\tau} \exp[-\frac{1}{2} \frac{(2\pi\tau)^2}{n}] d\tau \quad (4)$$

For an estimated ACF $\hat{R}_N(n)$ with finite data length N, $\hat{F}(\cdot)$ can also be estimated as follows:

$$\hat{F}(\lambda) \equiv \hat{F}([0, \lambda]) = \frac{1}{2\pi} \hat{R}_N(0)\lambda + \frac{1}{2\pi} \sum_{n=1}^{N} \hat{R}_N(n) \frac{2\sin(\lambda n)}{n}, \quad \text{where } \lambda \in [0, 2\pi). \quad (5)$$

In practical signal processing, this estimated $\hat{F}(\cdot)$ will be designated as the SDF in this paper. The interval $[0, 2\pi)$ is then partitioned at points $\frac{2\pi k}{N}$ for $k = 0, ..., N - 1$ in the following:

$$\hat{F}[k] = \hat{F}(\frac{2\pi k}{N}) = \frac{1}{2\pi} \hat{R}_N(0) \frac{2\pi k}{N} + \frac{1}{2\pi} \sum_{n=1}^{N} \hat{R}_N(n) \frac{2\sin(\frac{2\pi n k}{N})}{n}, \quad k = 0, ..., N - 1. \quad (6)$$

Spectral frequency is obtained by differencing the sampled SDF as follows.

$$\Delta\hat{F}[k] = \hat{F}(\frac{2\pi k}{N}) - \hat{F}(\frac{2\pi(k-1)}{N}), \quad k = 1, ..., N - 1 \text{ and } \Delta\hat{F}(0) = 0. \quad (7)$$

Appendix B: Legendre Polynomials

The Legendre polynomials are invoked here as the fundamental bases for representing the SDF (4, 7, 8). Legendre polynomials $P_n(x)$ are solutions to the Legendre differential equation. The polynomials obey the so-called orthogonal relationship

$$\int_{-1}^{1} P_n(x)P_m(x)dx = \frac{2}{2n+1}\delta_{mm} .$$

If $m = n$, $\delta_{mn} = 1$; otherwise, $\delta_{mn} = 0$. (8)

In this paper, $P_n(x)$ is sampled and only the intervals from 0 to 1 will be used. Due to symmetry of SDF at π, only $(N/2 + 1)$ points will be needed instead of N points. Hence, the coordinate value $x = 1$ for $P_n(x)$ corresponds to the position $k = N/2$ of SDF. Without loss of generality, we choose N to be an even number and the length $(N/2 + 1)$ is denoted by L. In this case, $\hat{F}[N/2]$ is normalized to 1. Hence, the normalized SDF is a non-decreasing, right-continuous, and bounded function with $\hat{F}[0] = 0$ and $\hat{F}[N/2] = 1$. In addition, the end points match $P_n(0) = 0$ and $P_n(1) = 1$ for odd n. The odd LP's still obey the orthogonal relationship for $x \in [0, 1]$.

Appendix C: Fractal Dimension Estimation

Here, the algorithm for estimating the fractal dimension is presented as follows. More details can be found in (3, 4, 7, 8). Since sampled EMG signals and differenced CMG signals can be modeled as discrete-time FGN, this algorithm starts from the theoretical ACF $r_H[k]$ for discrete-time FGN. Its formula is listed in (3). The $r_H[k]$ is used to create a database for estimating the fractal dimension of real physiological signals. The calculation of fractal dimension is divided into two parts. In the first part, a database using LP's in Appendix B is generated. In the second part, according to this database, the fractal dimension of real physiological signals is estimated.

The detailed steps of the first part are as follows:

Step 1. Initially, depending on the window-size and K (terms of odd LP's), we create a new database for fractal dimensions. For instance, when K is 3, we use $P_1(x)$, $P_3(x)$ and $P_5(x)$ to represent SDF.
Step 2. Increase H with increment 0.0001 from 0.
Step 3. For each H, calculate the ACF $r_H[n]$ and then its SDF $\hat{F}(\lambda)$.
Step 4. Fit $\hat{F}(\lambda)$ with K odd polynomials and get K fitting coefficients $\{a_i\}$.
Step 5. Save coefficients $\{a_i\}$ into the database.
Step 6. When H reaches 0.9999, we have obtained the whole database.

The detailed steps of the second part are as follows:

Step 1. Calculate the ACF $r[n]$ of the signal $x[n]$ and then its SDF $\hat{F}(\lambda)$.
Step 2. Fit $\hat{F}(\lambda)$ with K odd LP's and get K estimated coefficients.
Step 3. Evaluate distances between the estimated coefficients with coefficients $\{a_i\}$ in the database. Find the most suitable H by the least-square distance criterion.
Step 4. Setting $D = 2 - H$.

Acknowledgments

We would like to thank Ms. Wen-Ching Lin of Taichung Veterans General Hospital for performing the animal experiments and providing data for this paper. This work was supported in part under the Grant number NSC 97-2221-E-007-072 of NSC.

References

1. Campbell, M.F., Walsh, P.C. and Retik, A.B. Campbell's Urology. Philadelphia, PA: Saunders, 2002.
2. Chancellor, M.B. and de Groat, W.C. Intravesical capsaicin and resiniferatoxin therapy: spicing up the ways to treat the overactive bladder. *J. Urol*. 162: 3-11, 1999.
3. Chang, S., Hu, S.J. and Lin, W.C. Fractal dynamics and synchronization of rhythms in urodynamics of female Wistar rats. *J. Neurosci. Meth*. 139: 271-279, 2004.
4. Chang, S., Li, S.J., Chiang, M.J., Hu, S.J. and Hsyu, M.C. Fractal dimension estimation *via* spectral distribution function and its application to physiological signals. *IEEE Trans. Biomed. Eng*. 54: 1895-1898, 2007.
5. Chang, S., Mao, S.T., Hu, S.J., Lin, W.C. and Cheng, C.L. Studies of detrusor-sphincter synergia and dyssynergia during micturition in rats *via* fractional Brownian motions. *IEEE Trans. Biomed. Eng.* 47: 1066-1073, 2000.
6. Chang, S., Mao, S.T., Kuo, T.P., Hu, S.J., Lin, W.C. and Cheng, C.L. Fractal geometry in urodynamics of lower urinary tract. *Chinese J. Physiol*. 42: 25-31, 1999.
7. Chang, S., Hsyu, M.C., Cheng, H.Y. and Hsieh, S.H. Synergic coactivation of muscles in elbow flexion *via* fractional Brownian motion. *Chinese J. Physiol*. 51: 376-386, 2008.
8. Chang, S., Chiang, M.J., Li, S.J., Hu, S.J., Cheng, H.Y., Hsieh, S.H. and Cheng, C.L. The cooperative phenomenon of autonomic nervous system in urine storage for Wistar rats. *Chinese J. Physiol*. 52: 72-80, 2009.
9. Cheng, C.L., Ma, C.P. and de Groat, W.C. Effect of capsaicin on micturition and associated reflexes in chronic spinal rats. *Brain Res*. 678: 40-48, 1995.
10. de Groat, W.C., Downie, J.W., Levin, R.M., Long Lin, A.T., Morrison, J.F.B., Nishizawa, O., Steers, W.D. and Thor, K.D. Basic neurophysiology and neuropharmacology. In: Incontinence, edited by Abrams, P., Khoury, S. and Wein, A. Plymouth, UK: Plymouth Distributors Ltd, 1999, pp. 105-155.
11. de Seze, M., Wiart, L., Joseph, P.A., Dosque, J.P., Mazaux, J.M. and Barat, M. Capsaicin and neurogenic detrusor hyperreflexia: a double-blind placebo-controlled study in 20 patients with spinal cord lesions. *Neurourol. Urodyn*. 17: 513-523, 1998.
12. Doob, J.L. Stochastic Processes. New York: Wiley, 1953.
13. Embrechts, P. and Maejima, M. Selfsimilar Processes. Princeton:

Princeton University Press, 2002.
14. Feder, J. Fractals. New York and London: Plenum Press, 1988.
15. Fowler, C.J. Intravesical treatment of overactive bladder. *Urology* 55: 60-64, discussion 66, 2000.
16. Fowler, C.J., Beck, R.O., Gerrard, S., Betts, C.D. and Fowler, C.G. Intravesical capsaicin for treatment of detrusor hyperreflexia. *J. Neurol. Neurosurg. Psychiatry* 57: 169-173, 1994.
17. Glass, L. and Mackey, M.C. From Clocks to Chaos: The Rhythms of Life. Princeton, N.J.: Princeton University Press, 1988.
18. Gray, H., Standring, S., Ellis, H. and Berkovitz, B.K.B. Gray's Anatomy: The Anatomical Basis of Clinical Practice, 39th ed. Edinburgh; New York: Elsevier Churchill Livingstone, 2005.
19. Kolmogorov, A.N. Wienersche Spiralen und einige andere interessante Kurven im Hilbertschen Raum. *C.R. (Doklady) Acad. Sci. USSR* 16: 115-118, 1940.
20. Kruse, M.N., Belton, A.L. and de Groat, W.C. Changes in bladder and external urethral sphincter function after spinal cord injury in the rat. *Am. J. Physiol*. 264: R1157-R1163, 1993.
21. Lazzeri, M., Spinelli, M., Beneforti, P., Zanollo, A. and Turini, D. Intravesical resiniferatoxin for the treatment of detrusor hyperreflexia refractory to capsaicin in patients with chronic spinal cord diseases. *Scand. J. Urol. Nephrol*. 32: 331-334, 1998.
22. Lecci, A., Giuliani, S., Tramontana, M., Criscuoli, M. and Maggi, C.A. Multiple sites of action in the inhibitory effect of nociceptin on the micturition reflex. *J. Urol*. 163: 638-645, 2000.
23. Liu, S.C. and Chang, S. Dimension estimation of discrete-time fractional Brownian motion with applications to image texture classification. *IEEE Trans. Image Processing* 6: 1176-1184, 1997.
24. Mandelbrot, B.B. The Fractal Geometry of Nature. San Francisco: Freeman, 1982.
25. Paley, R.E.A.C. and Wiener, N. Fourier Transforms in the Complex Domain. vol. 19. American Mathematical Society Providence, R. I., 1934.
26. Seki, S., Sasaki, K., Fraser, M.O., Igawa, Y., Nishizawa, O., Chancellor, M.B., de Groat, W.C. and Yoshimura, N. Immunoneutralization of nerve growth factor in lumbosacral spinal cord reduces bladder hyperreflexia in spinal cord injured rats. *J. Urol*. 168: 2269-2274, 2002.
27. Shaker, H.S., Tu, L.M., Kalfopoulos, M., Hassouna, M., Dion, S. and Elhilali, M. Hyperreflexia of the urinary bladder: possible role of the efferent function of the capsaicin sensitive primary afferents. *J. Urol*. 160: 2232-2239, 1998.
28. Shefchyk, S.J. Sacral spinal interneurones and the control of urinary bladder and urethral striated sphincter muscle function. *J. Physiol*. 533: 57-63, 2001.
29. Voss, R.F. Fractals in nature: From characterization to simulation. In: The Science of Fractal Images, edited by Peitgen, H.O. and Saupe, D. New York: Springer-Verlag, 1988, pp. 21-70.
30. Wong, E. and Hajek, B. Stochastic Processes in Engineering Systems. New York: Springer-Verlag, 1985.
31. Yaglom, A.M. An Introduction to the Theory of Stationary Random Functions. Rev. English Dover ed. New York: Dover Pub., 1973.